Impact of noble-metals on the catalytic stability of cobalt nanoparticles for the acceptorless dehydrogenation of alcohols

Arnaud Viola, Maylis Peboscq, Jennifer Peron, Marion Giraud, Lorette Sicard, Raj Kumar Ramamoorthy, Brandon Azeredo, Sophie Nowak, Philippe Decorse, Guillaume Viau, et al.

▶ **To cite this version:**

Arnaud Viola, Maylis Peboscq, Jennifer Peron, Marion Giraud, Lorette Sicard, et al.. Impact of noble-metals on the catalytic stability of cobalt nanoparticles for the acceptorless dehydrogenation of alcohols. Catalysis Today, 2019, 333, pp.97 - 104. 10.1016/j.cattod.2018.05.036 . hal-03487191

HAL Id: hal-03487191
https://hal.science/hal-03487191v1

Submitted on 20 Dec 2021

HAL is a multi-disciplinary open access archive for the deposit and dissemination of scientific research documents, whether they are published or not. The documents may come from teaching and research institutions in France or abroad, or from public or private research centers.

L'archive ouverte pluridisciplinaire **HAL**, est destinée au dépôt et à la diffusion de documents scientifiques de niveau recherche, publiés ou non, émanant des établissements d'enseignement et de recherche français ou étrangers, des laboratoires publics ou privés.

Distributed under a Creative Commons Attribution - NonCommercial 4.0 International License

Version of Record: https://www.sciencedirect.com/science/article/pii/S0920586118306345
Manuscript_f3df8f0608d2b3dac9d559c6ef86ae90

Impact of noble-metals on the catalytic stability of cobalt nanoparticles for the acceptorless dehydrogenation of alcohols.

Arnaud Viola,[a] Maylis Peboscq,[a] Jennifer Peron,[a,*] Marion Giraud,[a] Lorette Sicard,[a] Raj Kumar Ramamoorthy,[b] Brandon Azeredo,[a] Sophie Nowak,[a] Philippe Decorse,[a] Guillaume Viau,[b] Jean-Yves Piquemal[a,*]

[a]ITODYS, Sorbonne Paris Cité, Univ. Paris Diderot, 15 rue Jean-Antoine de Baïf, 75013 Paris, France.

[b]LPCNO, Université de Toulouse, CNRS, INSA, UPS, 135 avenue de Rangueil, F-31077 Toulouse Cedex 4, France.

J.P.: jennifer.peron@univ-paris-diderot.fr

J.-Y. P.: jean-yves.piquemal@univ-paris-diderot.fr

Keywords: oxidation of alcohols, cobalt, molecular hydrogen, noble metal, acceptorless dehydrogenation.

Abstract

Three different types of unsupported Co catalysts are prepared by the polyol process and investigated for the oxidation of alcohols through an acceptorless dehydrogenation pathway: cobalt spheres with a predominantly face-centered cubic structure, pure cobalt nanorods and Ru-decorated cobalt nanorods, both with a hexagonal compact structure. All the catalysts display a high chemoselectivity for the oxidation of long-chain model alcohols since only secondary alcohols can be transformed into the corresponding ketones. Besides the ketone generated, the highly valuable hydrogen molecule is produced as the only by-product. Irrespective of the shape, similar high conversions and high selectivities are measured for the first catalytic tests. Nevertheless, when the three types of particles are recycled, significant differences in terms of catalytic stability and morphological evolution are observed. All the Co crystal habits are substantially modified during catalysis although well-isolated particles are recovered after three consecutive runs. The highest catalytic stability is found for Co nanorods decorated by Ru nanoparticles.

© 2018 published by Elsevier. This manuscript is made available under the CC BY NC user license
https://creativecommons.org/licenses/by-nc/4.0/

1. Introduction

Selective oxidation of alcohols into carbonyl compounds is one of the most important transformations in synthetic chemistry, but it remains a difficult task. In order to replace traditional methods that require the use of stoichiometric quantities of toxic oxidants such as chromium(VI) reagents, much attention has been paid to the development of catalysts using molecular oxygen as the oxidant [1]. Besides aerobic oxidations, another strategy corresponds to the so-called acceptorless dehydrogenation of alcohols (ADA). It is highly attractive from the viewpoint of atom economy since it avoids the use of hydrogen acceptors, such as O_2 or sacrificial carbonyl compounds or alkenes, and avoids the generation of organic and inorganic waste side-products [2]. Moreover, without a hydrogen acceptor, the highly valuable hydrogen molecule, considered to be the fuel of the future, is generated [3]. Although alcohol dehydrogenation is thermodynamically unfavorable at room temperature, the release of H_2 has a positive entropic contribution and therefore shifts the equilibrium favorably by removal of H_2 gas [3].

Different types of catalysts have been developed for ADA. Several studies were related to homogeneous catalysts, however, they generally require acid or base activation, necessitate the extensive synthesis of ligands and are difficult to separate and recycle [2, 4]. Heterogeneous catalysts such as Cu [5, 6] or Ag [7] supported on hydrotalcite, Ni/Al_2O_3 [25], Cu/Cr_2O_3 [26], Co/TiO_2 [15] or Ru/AlO(OH) [27] have also been widely investigated. Nevertheless, the support has a strong influence on the catalytic activity, impeding to assess the intrinsic activity of the metal nanoparticles (NPs) alone. Given the remarkable results obtained these last years with the preparation of size- and shape-controlled NPs, great expectations have been placed in the use of tailored NPs for catalytic applications. As far as structure sensitive reactions are considered, it is expected that a careful control of, not only the size, but also the shape of nanocrystals, is a way to enhance activities and selectivities. However, unsupported metal NPs have been hardly used for the ADA, selected examples corresponding to Re nanoparticles [8] or Mo_2N nanobelts [9]. Very often the sizes and shapes of unsupported nanoparticles are modified during catalysis leading to aggregates and/or agglomerates [10]. The use of shape controlled nanoparticles for catalysis is thus also an opportunity to assess the degradation mechanisms in recycling. Indeed, well isolated particles can be thoroughly studied in term of size, shape and structural evolution.

Recently, we have reported that during the synthesis of Co nanorods in 1,2-butanediol: i) a fraction of the diol was selectively oxidized into a keto-alcohol and ii) the concentration of the ketoalcohol continuously increased with time even after complete reduction of Co, suggesting a catalytic effect [11]. This was an incentive to evaluate the catalytic activity of unsupported Co

nanoparticles towards the acceptorless dehydrogenation of (poly)alcohols. The first obtained results indicated that Co particles were efficient catalysts for acceptorless dehydrogenation of mono-alcohols, with a very good chemoselectivity towards secondary alcohols compared to primary one [12]. Based on DFT calculations, a reaction pathway was proposed to account for the observed products, with firstly the formation of alkoxy and hydride surface species generated through the O-H bond cleavage of the alcohol. The surface alkoxy species then evolves into an adsorbed carbonyl compound with the formation of another hydride species. Finally, the carbonyl compound desorbs while the two hydride species combine to generate molecular hydrogen [12].

In this paper, we present the catalytic properties of unsupported Co particles prepared without and with noble metals seeds towards the oxidation of long-chain alcohols under solvent-free conditions. With two different seeding agents, $RuCl_3 \cdot xH_2O$ or $IrCl_3 \cdot xH_2O$, Ru-decorated and non-decorated Co nanorods are obtained respectively, while without seeds sub-micron Co spheres are recovered. Because of their ferromagnetic nature at room temperature, the particles are easily recovered from the reaction medium using an external magnetic field. A peculiar attention is directed towards the particles prepared with noble-metal seeds since these later can account for increased catalytic stability as well as activity.

2. Experimental

2.1. Chemicals

$Co(CH_3COO)_2 \cdot 4H_2O$ (Sigma Aldrich, > 98%), $RuCl_3 \cdot xH_2O$ (Aldrich, ref. 463779, 99.98%), $IrCl_3 \cdot xH_2O$ (Alfa Aesar, 99.8%), NaOH (Acros), 1,2-butanediol (Fluka, 98%), methanol (VWR, Normapur), dodecanoic acid, $C_{11}H_{23}COOH$ (Alfa Aesar, 99.5%), octan-2-ol (Merck, > 98%) and octan-1-ol (Merck, > 96%) were used without any further purification. The preparation of the $Co(C_{11}H_{23}COO)_2$ salt was described elsewhere.[13]

2.2. Catalyst preparation

Co nanospheres. Cobalt(II) dodecanoate (3.66 g, 80 mM) and sodium hydroxide (0.300 g, 75 mM) were added into 100 mL of 1,2-butanediol. The mixture was heated under stirring at 100 rpm to 448 K with a heating rate of 8 $K \cdot min^{-1}$ for half an hour until the color of the solution turned black, indicating the reduction of Co(II) into metallic cobalt. After cooling down to room temperature, the cobalt particles, denoted Co-S, were recovered using a permanent magnet, washed twice with absolute ethanol, and finally dried in an oven at 323 K.

Co nanorods prepared with Ru seeds. The synthesis was performed following the synthesis described above, except that $RuCl_3 \cdot xH_2O$ (42.5 mg, [Ru]/[Ru+Co] = 2.5 mol %) was added in the reaction mixture before the heating step. The particles, labeled Co-R-Ru, were recovered and washed as described above.

Co nanorods prepared with Ir seeds. The synthesis was performed as described above except that $IrCl_3 \cdot xH_2O$ was used instead of $RuCl_3 \cdot xH_2O$. The particles are labeled Co-R-Ir.

2.3. Catalyst characterizations

X-ray diffraction analyses were carried out using a Panalytical X'pert pro diffractometer equipped with a Co anode ($\lambda K\alpha$ = 1.7889 Å) and a X'celerator detector. The sizes of coherent diffraction domains were determined using MAUD software [14] which is based on the Rietveld method combined with Fourier analysis, well adapted for broadened diffraction peaks. Corrections for instrument broadening were made using a poly-crystalline silicon standard from Panalytical. The relative proportions of the Co hcp and fcc phases were determined using an already published procedure [15].

Routine transmission electron microscopy (TEM) characterizations were performed using a transmission electron microscope Tecnai 12 equipped with a CCD camera (SiS 1Kx1K Keen View), a LaB_6 filament and operating at 80 kV. All samples were prepared by evaporating a drop of diluted suspension in ethanol on a carbon-coated copper grid.

Scanning transmission electron microscopy coupled with high angle annular dark field imaging (HAADF-STEM) observations and local chemical analysis by energy dispersive spectroscopy (EDS) were performed on a probe corrected JEOL JEM-ARM200F instrument equipped with a cold field emission gun.

SEM-FEG images were obtained using a Zeiss SUPRA 40 FESEM, operating at 5 kV.

Physisorption studies were performed with N_2 at 77 K using a Belsorp-max apparatus from MicrotracBEL. Before analysis, the samples were outgassed at 423 K for 12 h under 0.1 Pa. The BET treatment [16] was carried out in the relative pressure range 0.05 – 0.25.

Elemental analyses of the powders were conducted by ICP-OES using an ICAP 6300 from ThermoElectron and by Energy Dispersive X-ray fluorescence (EDXRF) using an epsilon 3XL spectrometer from Panalytical equipped with a silver X-ray tube. As regard EDXRF, three measurement conditions give the opportunity to obtain the best signal-to-noise ratio for both the lightest element (Co) and the heaviest (Ir). The calibration has been performed by depositing a mass in the range 5-20 µg of the standard solution of each element on a polycarbonate membrane. The

same conditions have been adopted for all samples. The detection limits for Co, Ru and Ir were determined to be 10.2, 3.7 and 12.0 ng.

X-ray photoelectron spectroscopy (XPS) signals were recorded using a Thermo VG ESCALAB 250 system equipped with a microfocused, monochromatic Al Kα X-ray source (1486.6 eV) and a magnetic lens, which increases the electron acceptance angle and hence the sensitivity. A 650 µm sized X-ray beam was used at a power of 200 W (15 kV). The spectra were acquired in the constant analyzer energy mode, with a pass energy of 100 and 40 eV for the survey and the narrow regions, respectively. Charge compensation was achieved with an electron flood gun for insulating samples. The energy and emission current of the electrons were 4 eV and 0.15 to 0.20 mA, respectively. Avantage software, version 4.67, was used for data digital acquisition and processing. The peak binding energy positions were calibrated by setting the C 1s component due to hydrocarbon contamination at 285 eV.

2.4. Catalytic tests

For a typical test, Co nanoparticles were dispersed directly (i.e. without a solvent) in the long-chain alcohol substrate in a three-neck round-bottom flask equipped with a condenser and the suspension was heated to 453 K with the maximum possible heating rate delivered by a pre-heated heating mantle (about 5 min were necessary to reach the desired value of 453 K). For the Co nanorods (samples Co-R-Ru and Co-R-Ir), the alcohol/Co_{total} molar ratio was fixed to 150/1. For the Co-S sample, with a significantly lower specific surface area than the Co nanorods, the test was performed with a higher catalyst weight in order to operate with the same exposed metal surface area. For evaluation of the recyclability of the catalysts, the particles were recovered after 24h of reaction using a permanent magnet, washed with the substrate and reused under the same operating conditions. For the recycling experiments, we did not take into account the possible variations in specific surface areas that can occur during recycling. ICP-OES analyses were conducted on the filtrate to assess the possible leaching of metal species from the particles during catalysis. The results are given in ppm of Co, i.e. in mg of Co per kg of effluent. For each cycle, conversion and selectivity were determined as a function of time of reaction by recording ^{1}H NMR spectra of aliquots of the reaction medium and by comparing the integral of the signals of the alcohol to that of the corresponding ketone (see Figure S1 for an example with octan-2-ol). NMR spectra were recorded in $CDCl_3$ using a Bruker Avance III spectrometer operating at 400 MHz. The liquid samples were also analyzed using a Varian 450 Gas Chromatograph equipped with a 320 MS mass spectrometer and a VF-5MS column (5 wt.% biphenyl grafted polydimethylsiloxane; length 60 m, i.d. 0.25 mm). Gas aliquots were also taken during the course of the reaction. The nature and the purity of the

generated gas were assessed using a Hewlett-Packard 6890 series GC system with a thermal conductivity detector (2 m Agilent Technology 1/8'' Carbosieve S3 60−80 mesh column) and calibrated with pure H_2 gas. Finally, given the overall oxidation reaction of the alcohol: CH_3-CH(OH)-R' → CH_3-C(=O)-R' + H_2, conversion was also calculated by measuring the volume of generated H_2 using a Bronkhorst flow meter linked to a micro-computer. A schematic representation of the experimental setup is shown in Figure S2 (SI).

3. Results and discussion

3.1. Characterization of the catalysts

The Co nanometer-sized catalysts are prepared by the reduction of a long-chain carboxylate Co(II) precursor using a well-known soft chemistry method: the polyol process [17]. In this process, the polyol acts as the solvent, the growth medium and a mild reducing agent. For the cobalt growth by the polyol process, a small quantity of a noble metal can be added to the reaction mixture that will first be reduced. The so-generated noble metal particles will act as seeds for the cobalt growth. This seeded-growth method lowers the temperature at which the nucleation of these less-easily reducible metals starts and is a way to have a good control of the cobalt particle size and shape [15, 18, 19]. In this work, very different morphologies were obtained whether a seeding agent was present in the reaction medium or not: submicron-sized rough Co spheres were obtained in the absence of a noble metal seed (sample Co-S) and Co anisotropic nanometer-sized particles were obtained when using $RuCl_3.xH_2O$ and $IrCl_3.xH_2O$ as nucleating agents (samples Co-R-Ru and Co-R-Ir, respectively) (see Figure 1). The cobalt spheres are made of agglomerated small anisotropic objects and have a mean diameter of *ca.* 390 nm. Co-R-Ir particles display a much lower mean length ($<L_{TEM}>$) than that of Co-R-Ru, while the diameters ($<D_{TEM}>$) are comparable, resulting in a lower mean aspect ratio (AR = $<L_{TEM}>/<D_{TEM}>$) for the former (AR = 7) than for the latter (AR = 18). For these two anisotropic samples, high resolution TEM performed on microtomic slices (see Figure S3 for an example with Co-R-Ru, SI) reveals the exact nature of the particles exposed facets: 6 lateral $\{11\bar{2}0\}$ facets and 2 (0001) facets corresponding to the tips are observed. Because of the high anisotropy of the particles, it is reasonable to consider that the Co nanorods are mainly exposing $\{11\bar{2}0\}$ facets. Such a study was not possible for the Co spheres because of their obvious polycrystalline nature (see inset in Figure 1).

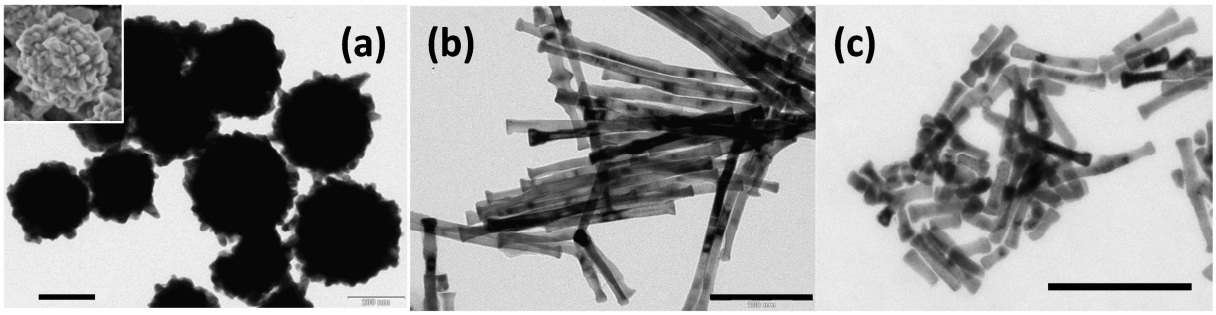

Figure 1. Transmission electron microscopy images of catalysts Co-S (a), Co-R-Ru (b) and Co-R-Ir (c). Inset: scanning electron microscopy image showing the surface roughness of the spheres. The scale bar stands for 200 nm.

The X-ray diffraction patterns of the nanoparticles are presented in Fig. 2. Samples Co-R-Ru and Co-R-Ir crystallize in the pure hexagonal system while the presence of superficial CoO can be hardly detected. It has previously been shown that for Co nanorods extracted from their synthesis medium, a very thin CoO oxide layer of about 1.5 nm is formed, protecting the rods from core oxidation [20]. By contrast, if the particles are kept in the synthetic mixture, no surface oxidation can be detected by magnetic measurements [20]. The Co particles prepared without a seeding agent crystallize mainly with the fcc structure (see Table 1), suggesting that the noble metal seeds formed in-situ act as chemically-heterogeneous nucleating agents and promote the development of the hexagonal phase. This interesting result necessitates further work but is obviously beyond the scope of this work.

Chemical analyses were performed by X-ray fluorescence (XRF) and inductively coupled plasma optical emission spectroscopy (ICP-OES) on samples Co-R-Ru and Co-R-Ir to ascertain the presence of the noble metal in the final product (see Table 1). For sample Co-R-Ru, both XRF and ICP-OES analyses gave very close results and revealed that Ru is present in the recovered material. However, the measured Ru/Co ratio is much lower than that in the initial material. Assuming that the seeds are incorporated in the Co particles, as previously proposed for Co-Ni-Fe alloys [19], these results suggest that not all the Ru precursors acted as seeds during the synthesis. For the materials prepared with $IrCl_3.xH_2O$, no Ir could be found by XRF (below the detection limit) while ICP-OES allowed to evidence Ir. Note that the Ir/Co ratio for sample Co-R-Ir is much lower than the Ru/Co ratio for sample Co-R-Ru. Moreover, the measured Ir/Co ratio is highly consistent with that

calculated assuming that one 2 nm sized seed is incorporated in one Co particle and using a simple geometrical model with the mean diameter and mean length measured by TEM.

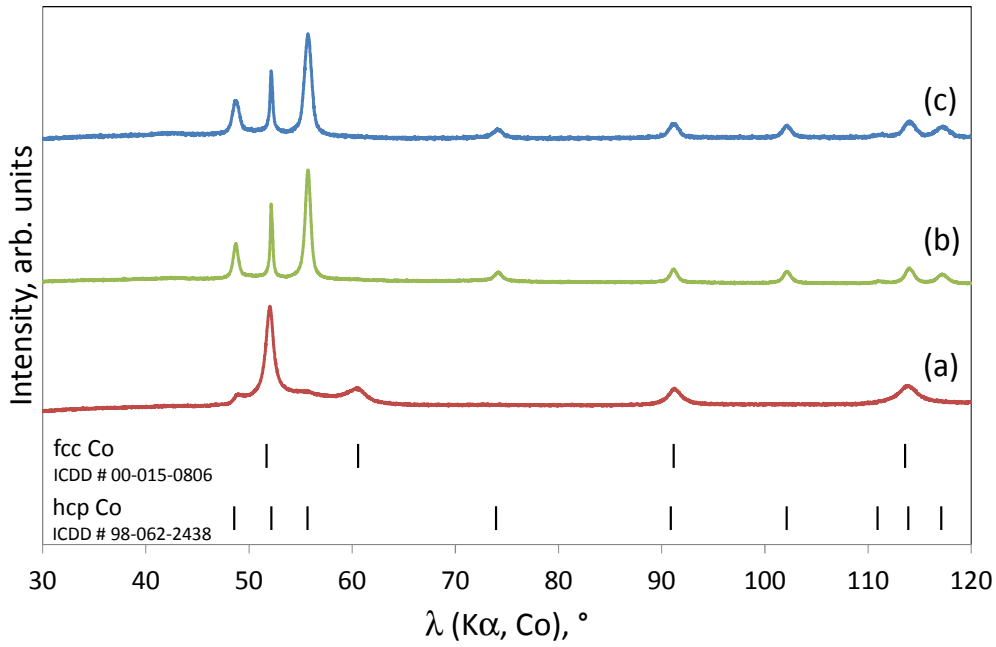

Figure 2. X-ray diffraction patterns of: Co spheres (a), Co nanorods prepared with Ru seeds (b) and Co nanorods prepared with Ir seeds (c).

To better characterize the surface of the anisotropic Co particles, XPS analyses were carried out on fresh samples as well as on samples after the first catalytic test. Figure 3 gathers the C 1s and Co 2p components centered at *ca.* 285 and 778-800 eV, respectively, as well as the high resolution spectra corresponding to the Ir 4p and Ru 3p regions after the first catalytic test for samples Co-R-Ir and Co-R-Ru, respectively. The Co $2p_{3/2}$ and $2p_{1/2}$ high-resolution spectra were fitted by taking into account signals corresponding to Co(0) and Co(II) with two types of contributions: $Co^{II}O$ as well as Co^{II} centers coordinated to $C_nH_{2n+1}COO^-$ species [21]. For native samples, note that the signal corresponding to Co(0) was hardly detected for the two samples (see Figure S4, SI). This is well-explained by the formation of a thin CoO layer for samples extracted from their reaction mixture, with adsorbed carboxylate ligands on top. Both are screening the cobalt metal that is evidenced by X-ray diffraction (see Figure 2). In contrast, the component associated with Co(0) was clearly observed for samples analyzed immediately after catalysis. This can be easily explained by the reducing ability of the alcohol [22]. Interestingly, the Co(0) signal was much more developed for sample Co-R-Ru than for sample Co-R-Ir. This will be discussed in section 3.3. As regards the C1s high-resolution spectrum, two peaks are seen for the two samples at about 285 and 289 eV that are respectively ascribed to

aliphatic carbon atoms and carbon atoms of the carboxylic group of the long-chain carboxylate ligands. A contribution at ca. 286 eV was also considered in the deconvolution; it is assigned to the carbon beta to the carboxylic function [23].The two observed peaks in the C 1s region are in agreement with what was reported previously for fatty acids interacting with Co NPs [24]. For sample Co-R-Ru, a broad signal located at *ca.* 461.6 eV is attributed to Ru $3p_{3/2}$ [25] and confirms the existence of Ru(0) in the sample. The (Ru/Co) molar ratio determined by XPS is much higher than the ratio determined by XRF or by ICP-OES, suggesting that Ru is mainly located at the surface of the rods. For the sample Co-R-Ir, no iridium could be detected in the binding energy range expected for the 4p3/2 component (see Figure 3f) revealing that the surface of Co-R-Ir is Ir-free.

Table 1. Physico-chemical features of the native cobalt nanometer-sized catalysts.

Sample	Seeding agent M	Co crystallographic phases	(M/Co), mol/mol[a] XPS	ICP-OES	XRF	S_{BET}, m^2/g
Co-S	None	8 % hcp, 92 % fcc	0	0	0	3.6
Co-R-Ru	Ru	100 % hcp	$2.0 \cdot 10^{-2}$	$2.0 \cdot 10^{-3}$	$2.3 \cdot 10^{-3}$	22.1
Co-R-Ir	Ir	100 % hcp	-[b]	$5.5 \cdot 10^{-4}$	-[b]	29.1

[a]the initial M/Co molar ratio is $2.5 \cdot 10^{-2}$ mol/mol; [b]below the detection limit (see experimental part).

Since XPS analyses revealed the presence of Ru in the Co-R-Ru sample, HAADF-STEM analyses were performed to locate Ru in the material. Whereas the bright field images of Co NRs do not show a clear contrast (not shown here), several white spots indicating the presence of heavier elements were seen on the dark field images (Figures 4a and 4b). Analysis performed on the edge of a rod clearly shows that the particles are lying at the particle surface (Figure 4b). Local EDS analysis confirmed that these white spots are tiny Ru nanoparticles (Figure 4c). To sum up, very tiny Ru NPs are thus evidenced at the surface of the Co rods after synthesis while the surface of sample Co-R-Ir is free of iridium.

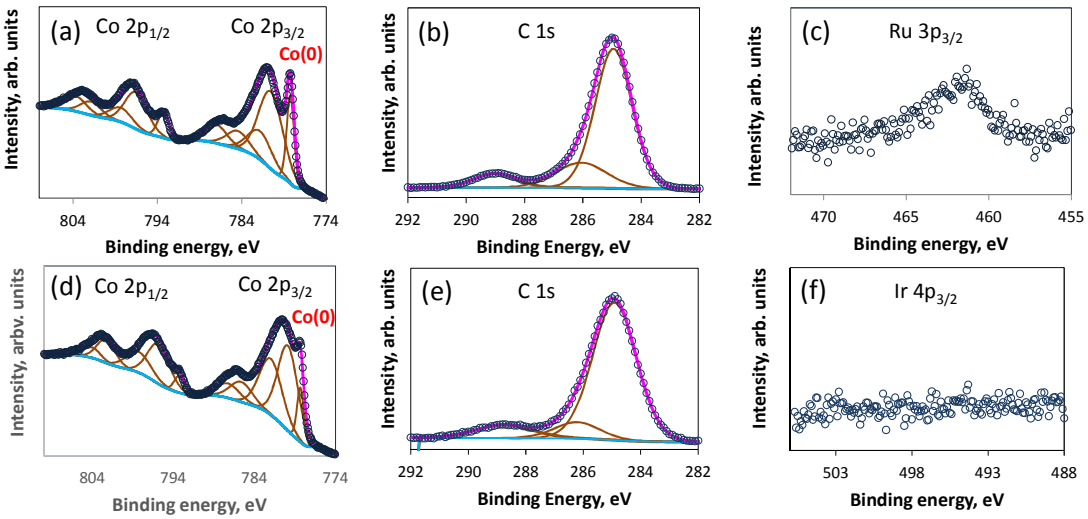

Figure 3. XPS spectra of Co-R-Ru (a, b, c) and Co-R-Ir (d, e, f) samples after the first catalytic test. The circle symbols correspond to the measured data while the line in pink, light blue and orange correspond respectively to the calculated profile, the background and the peak contributions.

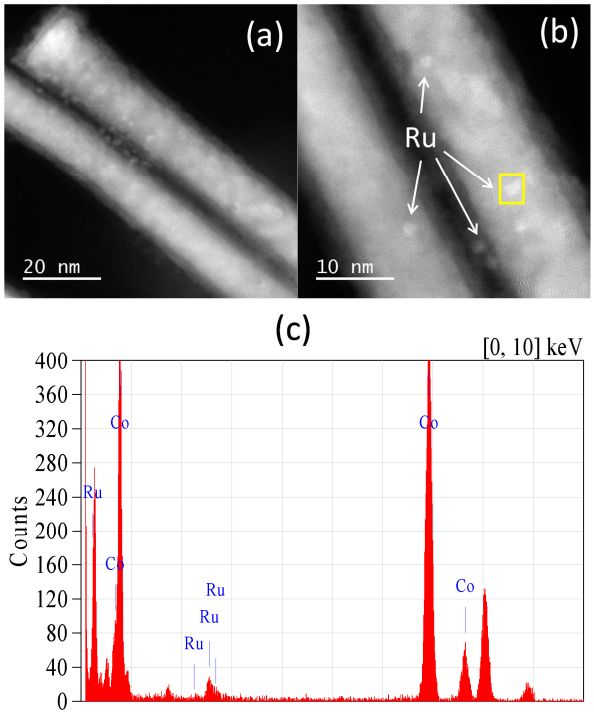

Figure 4. High-angle annular dark field (a,b) scanning transmission electron microscopy images of sample Co-R-Ru. (c) Energy dispersive X-ray analysis performed on the zone corresponding to the yellow rectangle in (b).

3.2. Acceptorless dehydrogenation of alcohols

Recently, we reported that unsupported Co particles were efficient catalysts for the acceptorless dehydrogenation of a variety of aliphatic and aromatic secondary alcohols [12]. In the present work, we show that the surface of Co particles prepared with Ru seeds is in fact decorated by tiny Ru NPs that could exert a significant influence on the activity and/or stability of the nano-catalysts. In contrast, there is no Ir at the surface of the Co-R-Ir sample. In order to evaluate the possible contribution of these noble metal Ru NPs on the activity and the stability of the Co particles, the three types of unsupported Co particles (Co-S, Co-R-Ru and Co-R-Ir) were tested under solvent-free conditions (i.e. the substrate only) towards the acceptorless dehydrogenation of two model alcohols: octan-2-ol and octan-1-ol. With the later, the conversion was always very low (inferior to 5%), irrespectively of the catalyst used. For the secondary alcohol, the catalysts display very good activities with conversions higher than 80 % after 24h at 453 K (see Figure 5). The same trend is observed for the three catalysts: conversion increases very rapidly during the first 5h hours then reaches a pseudo-plateau. During the course of the reaction, quasi-pure molecular hydrogen is evolved from the reaction medium (Figure 5d) and quantified by volumetric measurements. The obtained volumetric values match very well with those calculated by ^{1}H NMR indicating that the reaction proceeds through an acceptorless dehydrogenation mechanism. No significant difference in conversion after 24 h is found between the three sets of particles for the first test. Initial rates were calculated after 15 min reaction time: 1.40, 1.41 and 0.52 mmol·min^{-1}·m^{-2} were respectively found for samples Co-S, Co-R-Ru and Co-R-Ir. These results show that Co-S and Co-R-Ru display very close initial activities while that of Co-R-Ir is much lower. It is difficult to discuss on the activities of samples Co-S and Co-R-Ru since the two sets of particles exhibit very different shapes, sizes and crystal structures (pure hcp for Co-R-Ru, mainly fcc for Co-S). That is however not the case for the two anisotropic nanocatalysts. For Co-R-Ru sample, Ru NPs are located at the surface of the Co rods and could explain, at least partly, the observed higher initial activity. A catalytic test was thus performed test with the system $RuCl_3 \cdot xH_2O$/$Na(C_{11}H_{23}COO)$/octan-2-ol using the same conditions than that used for Co particles with a Ru amount similar to that found in the Co-R-Ru catalyst (Ru/Co = 2.0 10^{-3} mol/mol, see SI, Figure S5). In these conditions, Ru(III) species were reduced in Ru(0) NPs stabilized by dodecanoate ligands that have an average diameter of ca. 5 nm, as evidenced by TEM (see SI, Figure S5). But a very low activity (1.5 % conversion after 24 h) was observed, suggesting that the highest activity for Co-R-Ru compared to Co-R-Ir is mainly due to Co and not to the surface Ru NPs.

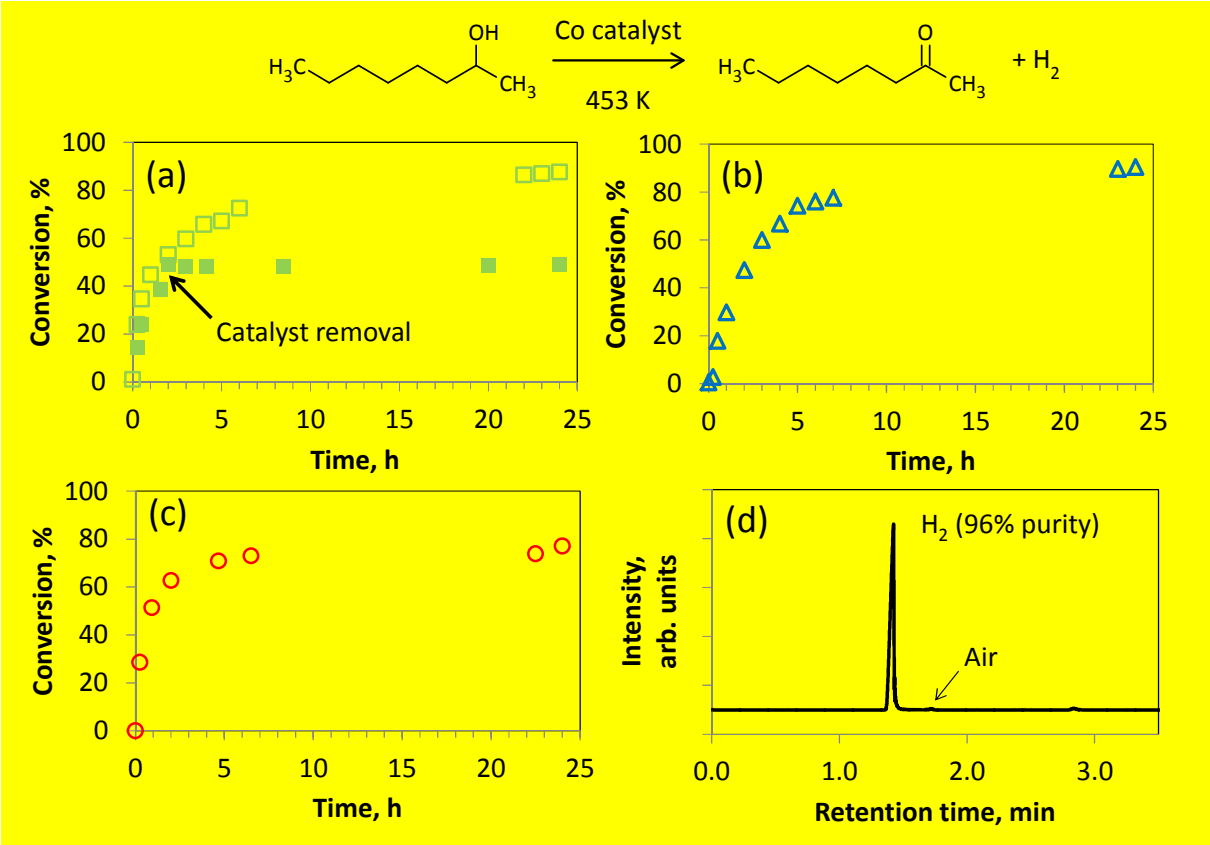

Figure 5. Conversion of octan-2-ol into octan-2-one determined by ^{1}H NMR as a function of time for samples: (a) Co-R-Ru (□) and Co-R-Ru with removal of the catalyst at 453 K after 2 h reaction time (■), (b) Co-R-Ir (△) and (c) Co-S (○). (d) Chromatogram of the gas phase after 5h reaction time obtained for the sample Co-R-Ru. Reaction conditions: T = 453 K, tests performed with the same exposed surface area (S_{Cata} = 0.44 m²), $V_{alcohol}$ = 8 mL, time = 24h.

3.3. Recycling experiments

For unsupported nanoparticles, the stability of the particle habitus is an important issue. Very often, important morphological evolutions are observed during catalysis that can affect the efficiency of the active phase [10]. Recycling experiments were thus performed using octan-2-ol as the model substrate in order to evaluate the catalytic stability as well as to monitor possible shape modifications. These recycling experiments were facilitated by the very good magnetic properties of the Co ferromagnetic particles: a simple permanent magnet was used to separate the particles from the reaction mixture avoiding tedious separation procedures. Results corresponding to the acceptorless dehydrogenation of octan-2-ol for the three Co catalysts are presented in Figure 6. A quite high (higher than 91 %) and constant selectivity is observed in the recycling experiments, irrespective of the catalyst used. However, marked differences can be observed as regards

conversions. For rough spheres, the conversion of 81 % after the first test drops significantly to 58 % then to 52 % after the second and the third, respectively. By contrast, with Co-R-Ru particles both the conversion and the selectivity remain very stable during three consecutive catalytic cycles, indicating a very good catalytic stability. For the third set of catalysts, anisotropic Co particles prepared with Ir seeds, a drop in conversion is also measured but to a lesser extent than for the sample Co-S. The highest stability is thus observed for the sample prepared with Ru seeds, which correspond to Co nanorods decorated with Ru nanoparticles. The observed drops in conversion could be explained, to some extent, by a decrease in specific surface area: variations were found to be 22, 12 and 24 % after the first test for samples Co-S, Co-R-Ru and Co-R-Ir, respectively. Nevertheless, it is noteworthy that a constant activity is found for sample Co-R-Ru suggesting that a decrease in specific surface area cannot entirely account for the observed decrease in activity. Since Co nanorods prepared using Ir seeds do not eventually contain Ir at the surface of the final products, above mentioned results suggest that Ru has a stabilizing effect. Such stabilizing effects have already been reported as regards Fischer-Tropsch catalysts. Indeed, it is commonly admitted that Ru, used as a promoter in Fisher-Tropsch Co catalysts, helps to reduce Co oxide species, i.e. catalyze cobalt reduction, presumably by hydrogen spillover from the promoter surface [26]. Here, the very good catalytic stability observed with the sample Co-R-Ru is explained by the presence of Ru nanoparticles at the surface helping to maintain and/or promote low oxidation states for surface Co atoms. This is in very good agreement with the XPS analyses performed on used samples that show that the Co(0) component is much more developed for Co-R-Ru than for Co-R-Ir (*vide supra*). Note that the interaction of these Ru NPs with the Co surface is sufficiently strong for the Ru/Co molar ratio to remain constant when the material is recycled (see Table 2). The results obtained with noble metal-free samples Co-S and Co-R-Ir, also suggest that the anisotropic shape and/or the hcp phase of Co is more favorable to keep a constant catalytic activity, since the highest drop in conversion is observed for the rough spheres that crystallize mainly with the fcc structure.

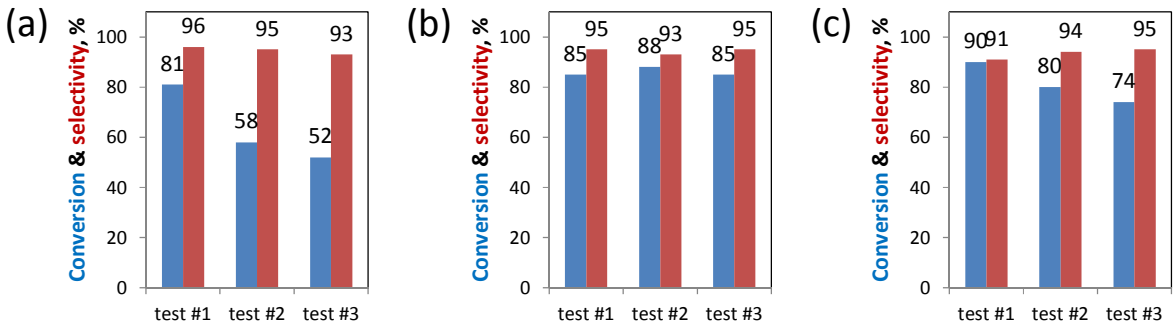

Figure 6. Conversion (blue) of octan-2-ol and selectivity (red) towards octan-2-one over Co nanospheres (a), Co nanorods prepared with Ru seeds (b) and Co nanorods prepared with Ir seeds (c) after the first, second and third catalytic tests. Reaction conditions: T = 453 K, tests performed with the same exposed surface area (S_{Cata} = 0.44 m²), $V_{alcohol}$ = 8 mL, time = 24h.

Table 2. M/Co (M = Ru, Ir) molar ratio determined by XRF analysis for the spent catalysts.

	$(M/Co)_{XRF}$, mol/mol		
Sample	**1st test**	**2nd test**	**3rd test**
Co-S	0	0	0
Co-R-Ru	$1.8 \cdot 10^{-3}$	$2.0 \cdot 10^{-3}$	$2.1 \cdot 10^{-3}$
Co-R-Ir	-[a]	-[a]	-[a]

[a]below the detection limit (see experimental part).

The measured drops in conversion for samples Co-S and Co-R-Ir are by far the most important after the first test. On the one hand, this could result from morphological evolutions leading to modifications in the nature and number of surface active sites. On the other hand, the stable activity obtained for sample Co-R-Ru does not necessarily mean that the particle shape is unmodified during catalysis. All catalysts were thus recovered from the reaction mixture and fully characterized. The XRD patterns of all the catalysts before and after the first catalytic test are very similar (see Figure S6, SI) showing no noticeable phase transformation or oxidation of the material. SEM image displayed in Figure 7a shows that there is a clear smoothing of the spheres surface for sample Co-S after the first catalytic test (see also Figure 1a for comparison purposes, images corresponding to the samples after the 2nd and 3rd tests are given in Figure S7, SI). This morphological evolution can be explained by a dissolution – reprecipitation mechanism, since chemical analyses of the liquid phase revealed that the Co amount is inferior to 1 ppm (corresponding to 0.04 % of the Co introduced in the reaction medium) after the first test. This surface reorganization modifies the

relative proportions of Co active sites such as kink and step atoms, explaining the observed decrease in activity. SEM analyses of samples Co-R-Ru and Co-R-Ir do not show noticeable modifications of the particle shape and anisotropic particles can still be observed. A detailed analysis of the microscopy data implying statistical studies on the lengths and diameters of the particles has been performed and is reported in Figure 8. It shows that the initial mean length and diameters of Co-R-Ru are larger than that of Co-R-Ir. There is a continuous decrease in the mean length and in the standard deviation of the particle length for the Co-R-Ru sample when it is recycled. At the same time, the decrease in length is accompanied with a slight increase in the rods diameter. The same trend is observed for Co-R-Ir even if the effect is less pronounced with this sample. As for Co-S catalysts, chemical analysis of the liquid solution did not reveal the presence of Co in solution, the decrease in length of the rods is not due to a mere rod dissolution but these morphological changes likely originate from an internal reorganization process. The evolution of the initial rods into smaller rods is probably based on a dissolution-reprecipitation mechanism in which Co atoms or Co(II) ions migrate from some "weak" points (or defects) and from the tips towards the lateral $\{11\bar{2}0\}$ facets. This process accounts both for the decrease in the particle length and the increase in the mean diameter. This morphological evolution is neither prevented nor facilitated by the presence of the noble-metal at the particles surface since it is observed for both types of materials, i.e. Co-R-Ru and Co-R-Ir. Nevertheless the presence of the Ru particles at the surface of the Co-R-Ru sample might facilitate the reduction of Co(II) ions into Co(0) on lateral facets; it allows the catalytic activity to be maintained.

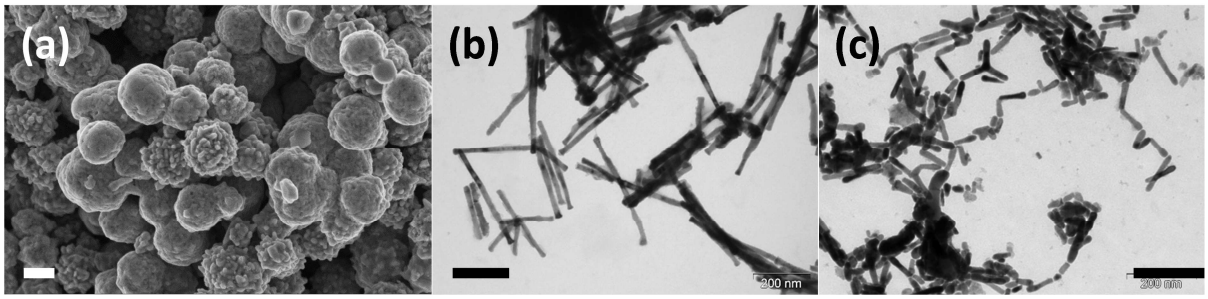

Figure 7. SEM (a) and TEM (b,c) images of samples Co-S (a), Co-R-Ru (b) and Co-R-Ir (c) recovered after the first catalytic test. The scale bar stands for 200 nm.

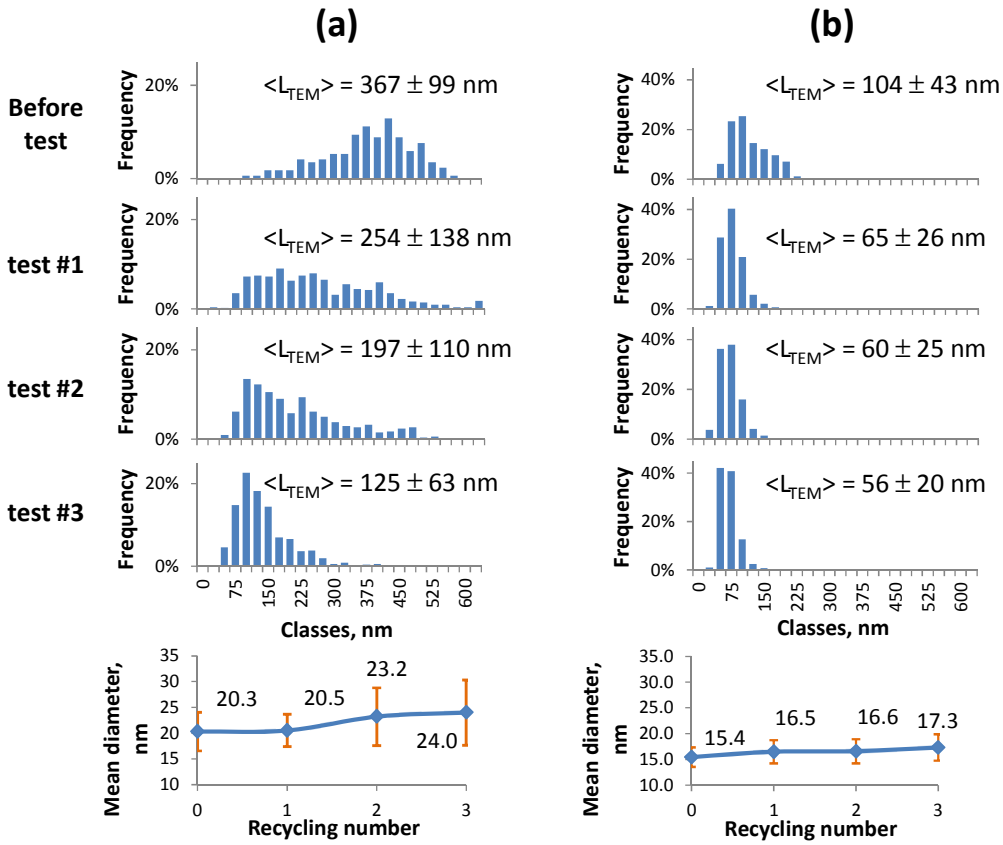

Figure 8. Distribution of length sizes for the native particles and after catalytic tests and evolution of the mean diameter for samples Co-R-Ru (a) and Co-R-Ir (b).

4. Conclusion

Depending on the presence or absence of noble metal seeds in the reaction mixture, cobalt particles with different shapes and crystal structures are prepared. In the presence of a seeding agent ($RuCl_3 \cdot xH_2O$ or $IrCl_3 \cdot xH_2O$), anisotropic nanometer-sized particles that crystallize with the hcp structure are generated while in the absence of seeding agent, sub-micrometer sized rough spheres with predominantly the fcc structure are isolated. In the case of the anisotropic particles, Ru NPs are present at the surface of the Co nanorods prepared with $RuCl_3 \cdot xH_2O$, while no Ir can be detected at the surface of the catalyst prepared using $IrCl_3 \cdot xH_2O$ as a seeding agent. The three sets of catalysts are active towards the acceptorless dehydrogenation of octan-2-ol into octan-2-one with very good selectivity and conversion. As regards anisotropic particles, Co catalysts decorated with Ru NPs show the highest initial activity, compared to Co particles with a noble-metal free surface. The presence of Ru nanoparticles at the surface of the Co rods is also of high importance regarding the catalytic recyclability. Among the three sets of Co particles, only the sample decorated with Ru particles shows

a stable conversion after three consecutive tests. This is explained by a promoting effect of Ru, favoring the reduction of surface Co(II) species into Co(0) ones, as proposed for Fischer-Tropsch Co-based catalysts. Because of the very good observed chemoselectivity for secondary alcohols compared to primary ones, work is in progress to assess the activity of these cobalt particles for bio-sourced poly-alcohol substrates such as glycerol.

Acknowledgements

The authors are indebted to Dr. Mickaël Sicard for GC-MS experiments. They also would like to thank L. Datas and T. Hungria (Plateforme Castaing, Toulouse, France) for the HAADF-STEM experiments and G. Le Faucheur and M.-E. Pinart from the service de TP de Chimie de l'Université Paris Diderot for the ICP-OES experiments. This work was funded by the French National Research Agency, ANR, in the framework of the TANOPOL project (ANR-15-CE07-0011-01).

References

[1] R.A. Sheldon, I.W.C.E. Arends, A. Dijksman, New developments in catalytic alcohol oxidations for fine chemicals synthesis, Catal. Today 57 (2000) 157-166.
[2] C. Gunanathan, D. Milstein, Applications of Acceptorless Dehydrogenation and Related Transformations in Chemical Synthesis, Science 341 (2013) 1229712.
[3] T.C. Johnson, D.J. Morris, M. Wills, Hydrogen generation from formic acid and alcohols using homogeneous catalysts, Chem. Soc. Rev. 39 (2010) 81-88.
[4] A. Friedrich, S. Schneider, Acceptorless dehydrogenation of alcohols: Perspectives for synthesis and H2 storage, ChemCatChem 1 (2009) 72-73.
[5] D. Damodara, R. Arundhathi, P.R. Likhar, Copper Nanoparticles from Copper Aluminum Hydrotalcite: An Efficient Catalyst for Acceptor- and Oxidant-Free Dehydrogenation of Amines and Alcohols, Advanced Synthesis & Catalysis 356 (2014) 189-198.
[6] T. Mitsudome, Y. Mikami, K. Ebata, T. Mizugaki, K. Jitsukawa, K. Kaneda, Copper nanoparticles on hydrotalcite as a heterogeneous catalyst for oxidant-free dehydrogenation of alcohols, Chem. Commun. (2008) 4804-4806.
[7] T. Mitsudome, Y. Mikami, H. Funai, T. Mizugaki, K. Jitsukawa, K. Kaneda, Oxidant-free alcohol dehydrogenation using a reusable hydrotalcite-supported silver nanoparticle catalyst, Angew. Chem. Int. Ed. 47 (2008) 138-141.
[8] J. Yi, J.T. Miller, D.Y. Zemlyanov, R. Zhang, P.J. Dietrich, F.H. Ribeiro, S. Suslov, M.M. Abu-Omar, A Reusable Unsupported Rhenium Nanocrystalline Catalyst for Acceptorless Dehydrogenation of Alcohols through γ-C–H Activation, Angew. Chem. Int. Ed. 53 (2014) 833-836.
[9] Z. Li, C. Chen, E. Zhan, N. Ta, W. Shen, Mo2N nanobelts for dehydrogenation of aromatic alcohols, Catal. Commun. 51 (2014) 58-62.
[10] A.P. Umpierre, E. de Jesús, J. Dupont, Turnover Numbers and Soluble Metal Nanoparticles, ChemCatChem 3 (2011) 1413-1418.

[11] K. Aït Atmane, C. Michel, J.-Y. Piquemal, P. Sautet, P. Beaunier, M. Giraud, M. Sicard, S. Nowak, R. Losno, G. Viau, Control of the anisotropic shape of cobalt nanorods in the liquid phase: from experiment to theory... and back, Nanoscale 6 (2014) 2682-2692.
[12] A. Viola, J. Peron, K. Kazmierczak, M. Giraud, C. Michel, L. Sicard, N. Perret, P. Beaunier, M. Sicard, M. Besson, J.-Y. Piquemal, Unsupported shaped cobalt nanoparticles as efficient and recyclable catalysts for the solvent-free acceptorless dehydrogenation of alcohols, Catalysis Science & Technology 8 (2018) 562-572.
[13] K. Gandha, K. Elkins, N. Poudyal, X. Liu, J.P. Liu, High Energy Product Developed from Cobalt Nanowires, Sci. Reports 4 (2014) 5345.
[14] L. Lutterotti, S. Matthies, H.R. Wenk, "MAUD: a friendly Java program for material analysis using diffraction.", IUCr: Newsletter of the Commission on Powder Diffraction, Proceeding of the Twelfth International Conference on Textures of Materials (ICOTOM-12), 1999, pp. 14.
[15] N. Chakroune, G. Viau, C. Ricolleau, F. Fiévet-Vincent, F. Fiévet, Cobalt-based anisotropic particles prepared by the polyol process, J. Mater. Chem. 13 (2003) 312-318.
[16] S. Brunauer, P.H. Emmett, E. Teller, Adsorption of Gases in Multimolecular Layers, J. Am. Chem. Soc. 60 (1938) 309-319.
[17] F. Fiévet, R. Brayner, The polyol process, in: R. Brayner, F. Fiévet, T. Coradin, (Eds.), Springer, 2012, pp. 1-28.
[18] Y. Soumare, C. Garcia, T. Maurer, G. Chaboussant, F. Ott, F. Fiévet, J.-Y. Piquemal, G. Viau, Kinetically Controlled Synthesis of Hexagonally Close-Packed Cobalt Nanorods with High Magnetic Coercivity, Adv. Funct. Mater. 19 (2009) 1971-1977.
[19] P. Toneguzzo, G. Viau, O. Acher, F. Fiévet-Vincent, F. Fiévet, Monodisperse Ferromagnetic Particles for Microwave Applications, Adv. Mater. 10 (1998) 1032-1035.
[20] T. Maurer, F. Zighem, F. Ott, G. Chaboussant, G. André, Y. Soumare, J.-Y. Piquemal, G. Viau, C. Gatel, Exchange bias in Co/CoO core-shell nanowires: Role of antiferromagnetic superparamagnetic fluctuations, Phys. Rev. B 80 (2009) 064427.
[21] Y. Okamoto, H. Nakano, T. Imanaka, S. Teranishi, X-ray Photoelectron Spectroscopic Studies of Catalysts - Supported Cobalt Catalysts -, Bull. Chem. Soc. Jpn. 48 (1975) 1163-1168.
[22] J.L.C. Huaman, N. Hironaka, S. Tanaka, K. Shinoda, H. Miyamura, B. Jeyadevan, Size-controlled monodispersed nickel nanocrystals using 2-octanol as reducing agent, CrystEngComm 15 (2013) 729-737.
[23] S.D. Techane, L.J. Gamble, D.G. Castner, Multi-technique Characterization of Self-assembled Carboxylic Acid Terminated Alkanethiol Monolayers on Nanoparticle and Flat Gold Surfaces, J. Phys. Chem. C 115 (2011) 9432-9441.
[24] N. Wu, L. Fu, M. Su, M. Aslam, K.C. Wong, V.P. Dravid, Interaction of Fatty Acid Monolayers with Cobalt Nanoparticles, Nano Lett. 4 (2004) 384-386.
[25] D.J. Morgan, Resolving ruthenium: XPS studies of common ruthenium materials, Surf. Interf. Anal. 47 (2015) 1072-1079.
[26] G. Jacobs, T.K. Das, Y. Zhang, J. Li, G. Racoillet, B.H. Davis, Fischer–Tropsch synthesis: support, loading, and promoter effects on the reducibility of cobalt catalysts, Appl. Catal. A 233 (2002) 263-281.

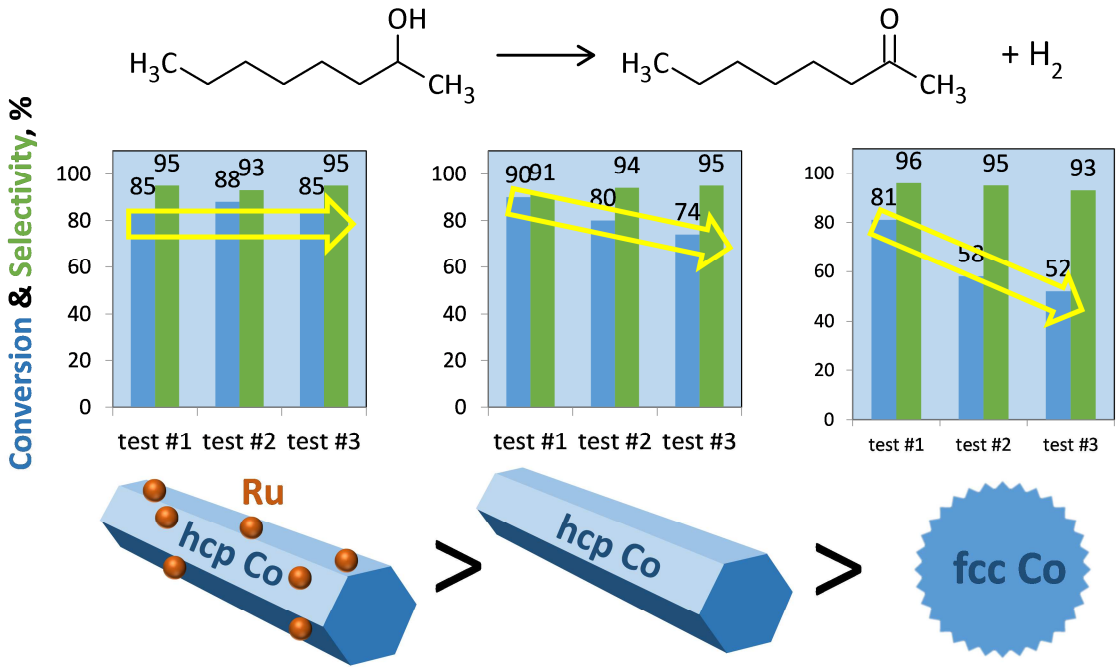
OH
H_3C
CH_3
O
H_3C
CH_3
+ H_2
Conversion & Selectivity, %
100
80
60
40
20
0
95
85
88
93
85
95
test #1
test #2
test #3
90
91
80
94
74
95
test #1
test #2
test #3
81
96
58
95
52
93
test #1
test #2
test #3
Ru
hcp Co
>
hcp Co
>
fcc Co